

1 **Discovery of compounds inhibiting the ADP-ribosyltransferase activity of pertussis toxin**

2

3 Yashwanth Ashok^{a,#}, Moona Miettinen^{b,c,#}, Danilo Kimio Hirabae de Oliveira^a, Mahlet Z.
4 Tamirat^d, Katja Näreoja^b, Avlokita Tiwari^b, Michael O. Hottiger^e, Mark S. Johnson^d, Lari
5 Lehtiö^{a,*} & Arto T. Pulliainen^{b,*}

6

7 ^aFaculty of Biochemistry and Molecular Medicine, Biocenter Oulu, University of Oulu, Oulu,
8 Finland

9 ^bInstitute of Biomedicine, Research Center for Cancer, Infections, and Immunity, University of
10 Turku, Turku, Finland

11 ^cTurku Doctoral Programme of Molecular Medicine (TuDMM), University of Turku, Turku,
12 Finland

13 ^dStructural Bioinformatics Laboratory, Biochemistry, Faculty of Science and Engineering, Åbo
14 Akademi University, Turku, Finland

15 ^eDepartment of Molecular Mechanisms of Disease, University of Zurich, Zurich, Switzerland

16

17 [#] Equal contribution

18

19 ^{*} Corresponding authors: lari.lehtio@oulu.fi, arto.pulliainen@utu.fi

20

21

22

23

24

25 Corresponding author information:

26

27 Dr. Lari Lehtiö, Ph.D.

28 Faculty of Biochemistry and Molecular Medicine & Biocenter Oulu, University of Oulu, Aapistie

29 7 B, FI-90220, Oulu, Finland

30 Phone: +358-2-9448 1169, Fax: not available, E-mail: lari.lehtio@oulu.fi

31

32 Arto Pulliainen, Ph.D.

33 Institute of Biomedicine, Research Center for Cancer, Infections, and Immunity, University of

34 Turku, Kiinamylynkatu 10, FI-20520, Turku, Finland

35 Phone: +358-40-1586044, Fax: not available, E-mail: arto.pulliainen@utu.fi

36

37 **RUNNING TITLE**

38 Inhibitory compounds for pertussis toxin

39

40

41

42

43

44

45

46

47

48

49 **ABSTRACT**

50 *Bordetella pertussis* causes the highly contagious respiratory disease pertussis, also known as
51 whooping cough. The resurgence of pertussis has been witnessed even in highly vaccinated
52 populations, and macrolide-resistant strains have been isolated. One attractive target for drug
53 development is the pertussis toxin – an important type IV secretion system-dependent virulence
54 factor of *B. pertussis*. The AB₅-topology pertussis toxin is composed of a pentameric PtxS2-S5
55 (1:1:2:1) complex mediating toxin binding to cell surface receptors, and one ADP-
56 ribosyltransferase subunit PtxS1. Once internalized into the host cell, PtxS1 ADP-ribosylates α -
57 subunits of heterotrimeric G α i-superfamily members, thereby disrupting G-protein-coupled
58 receptor (GPCR) signaling. Here, we describe protocols to purify mg-levels of truncated but
59 highly active recombinant *B. pertussis* PtxS1 from *E. coli* and an *in vitro* high throughput-
60 compatible assay to quantify NAD⁺ consumption during PtxS1-catalyzed G α i ADP-ribosylation.
61 The *in vitro* NAD⁺ consumption assay was used to screen compounds inhibiting the PtxS1
62 activity. Two inhibitory compounds (NSC 29193 and NSC 228155) with low micromolar IC₅₀-
63 values were identified that also were potent in an independent *in vitro* assay monitoring
64 conjugation of ADP-ribose to G α i. Docking and molecular dynamics simulations identified
65 plausible binding poses of NSC 228155 and in particular NSC 29193, most likely owing to the
66 rigidity of the latter ligand, at the NAD⁺-binding pocket of PtxS1. NSC 228155 inhibited the
67 pertussis AB₅ holotoxin-catalyzed ADP-ribosylation of G α i in living human cells in low
68 micromolar concentration. NSC 228155 and NSC 29193 might prove useful as lead compounds
69 in targeted drug development in pertussis.

70

71

72 INTRODUCTION

73 Pertussis, i.e. whooping cough, is a globally distributed acute respiratory disease (1). Pertussis
74 affects all age groups. However, young children are the most affected age group where pertussis
75 may lead to death despite hospital intensive care and use of antibiotics. Worldwide estimates of
76 pertussis cases and deaths in children younger than 5 years in 2014 were 24.1 million and
77 160.700, respectively (2). Despite efficient global vaccine campaign pertussis remains endemic
78 and recent data, e.g. from USA (3), indicate that the number of pertussis cases is increasing.
79 Sizeable outbreaks have also been reported (1), but the reasons for the resurgence of pertussis are
80 incompletely understood. On the one hand, improved diagnostics and surveillance methods as
81 well as increased awareness of pertussis by health care professionals might contribute (1). On the
82 other hand, molecular changes in the pathogenic *B. pertussis* lineages and waning immunity
83 especially after receipt of acellular pertussis vaccines have been extensively debated (1). These
84 data highlight the need to improve the vaccine formulations and vaccination campaigns, but also
85 to develop alternative means to treat pertussis.

86 Pertussis toxin is included in the acellular pertussis vaccine formulations in a detoxified form
87 (1), and has provided good protection even as a single component (4). At the same time, clinical
88 isolates lacking pertussis toxin, i.e. vaccine escape mutants, have turned out to be extremely rare
89 (5). Indeed, pertussis toxin is considered as a major virulence factor of *B. pertussis* (6, 7). When
90 administrated systemically to experimental animals, e.g. to mice (8), pertussis toxin recapitulated
91 the leukocytosis (increase in number of circulating white blood cells) seen in young children with
92 pertussis (1). Rats experimentally infected with *B. pertussis* developed paroxysmal coughing
93 lasting several days, but an isogenic pertussis toxin-deficient strain did not cause such pathology
94 (9, 10). Seven-day-old neonatal mice infected with a pertussis toxin-deficient strain of *B.*
95 *pertussis* fully survived a challenge, which caused 100% mortality with the parental strain (11).

96 Therefore, targeting of pertussis toxin might prove beneficial in the treatment of pertussis,
97 especially in young children who still lack the vaccine-induced protection against pertussis.

98 Pertussis toxin is composed of five non-covalently bound subunits (PtxS1-S5), which are
99 arranged in an AB₅-topology (12, 13). The B₅-assembly is formed by the PtxS2-S5 subunits
100 (PtxS2, PtxS3, 2 copies of PtxS4, PtxS5) (12, 13). Pertussis toxin is secreted from the bacteria via
101 Sec-pathway and Ptl type IV secretion system (14). The B₅-assembly mediates binding of the
102 secreted AB₅ holotoxin on the surface of various different cell types in a carbohydrate-dependent
103 manner (13). Subsequent cell entry is followed by dissociation of the B₅-assembly and the PtxS1-
104 subunit (15), which belongs to the family of ADP-ribosyltransferases (16). PtxS1 ADP-
105 ribosylates a single C-terminal cysteine residue in α -subunits of most heterotrimeric G α i-
106 superfamily members such as G α i, G α o, and G α t (17-19). The C-terminus of the heterotrimeric
107 G-protein α -subunits makes functionally important contacts with the plasma membrane-localized
108 G-protein coupled receptors (GPCRs) (20). Therefore, the bulky PtxS1-catalyzed ADP-ribose
109 modification decouples the G-protein α i-subunit from the GPCRs and inhibits signal propagation
110 initiated upon agonist stimulation of GPCRs.

111 Seven-day-old neonatal mice infected with a *B. pertussis* strain expressing a catalytically
112 inactive mutant of PtxS1 fully survived a challenge, which causes 100% mortality with the
113 parental strain of *B. pertussis* (11). Purified AB₅ holotoxin containing the same PtxS1 mutant is
114 incapable of inducing leukocytosis in mice in doses that are 100-fold more than the median lethal
115 dose of wild-type AB₅ holotoxin (21). It appears, therefore, that the enzymatic activity of PtxS1
116 is important for the pathological effects of pertussis toxin. In this study, we set out to identify
117 small molecular weight compounds inhibiting the G α i-specific ADP-ribosyltransferase activity of
118 pertussis toxin, and thereby to interfere with the cellular effects of pertussis toxin.

119

120 **RESULTS**

121 **Purification of recombinant PtxS1 from *E. coli*** – We did not succeed in purifying the full
122 length N- or C-terminally HIS-tagged recombinant PtxS1 from *E. coli* due to weak solubility and
123 proteolytic instability (data not shown). Therefore, we engineered a double deletion to *ptxA*
124 resulting into expression of an N-terminally HIS-tagged version of *B. pertussis* Tohama I strain
125 PtxS1 (UniProt_P04977), referred hereafter to as rPtxS1, which lacks the N-terminal secretion
126 signal sequence as well as part of the C-terminus (Fig. 1, Fig. 2A). The C-terminal truncation
127 exposes the ADP-ribosyltransferase (ART) catalytic site of PtxS1 including the NAD⁺-binding
128 pocket (Fig. 1)(12, 13). Structural data of the pertussis AB₅ holotoxin demonstrate that the C-
129 terminus of PtxS1 masks the active site, and indicate that di-sulfide bond reduction and
130 significant movement of the C-terminus would be required for catalysis (12, 13).

131 rPtxS1, as purified with metal affinity and size exclusion chromatography, is proteolytically
132 stable and migrates between the 25 and 20 kDa protein markers in SDS-PAGE (Fig. 2B), in
133 accordance with a theoretical size of 23.4 kDa. In order to study the oligomerization state of
134 rPtxS1 in solution, size exclusion chromatography coupled to static light scattering (SEC-MALS)
135 was used. Purified rPtxS1 appeared as a single peak (Fig. 2C), with an estimate of 23.04 ± 0.2
136 kDa in a triplicate run indicating that rPtxS1 is monomeric in solution. rPtxS1 is well folded as
137 evidenced by a sigmoidal curve with a melting temperature (T_m) of 51°C in a differential
138 scanning fluorimetry (DSF)-assay (Fig. 2D).

139
140 **Analysis of the ART activity of rPtxS1** – ART activity of rPtxS1 towards G α i was first studied
141 with a HEK293T cell membrane preparation having an endogenous level of G α i in an NAD⁺-
142 biotin Western blot-assay. rPtxS1 ADP-ribosylated one major protein from the complex

143 membrane proteome (Fig. 2E). This protein migrated between the 55 and 35 kDa protein markers
144 in SDS-PAGE (Fig. 2E), in accordance with a theoretical size of endogenous *Gai*, e.g. 40.4 kDa
145 for isoform 1 (UniProt_P63096). Next, ART activity of rPtxS1 towards *Gai* was studied with
146 recombinant N-terminally HIS-tagged *Gai* (isoform 1, UniProt_P63096) purified from *E. coli*,
147 hereafter referred to as r*Gai*, in an NAD⁺ Western blot-assay. rPtxS1 ADP-ribosylated r*Gai* (Fig.
148 2F), indicating that *Gai* may efficiently serve as a substrate without the G-protein $\beta\gamma$ -complex or
149 other cellular constituents. SEC-analysis of rPtxS1-r*Gai* complex solution topology shows the
150 presence of only single monomeric rPtxS1 and r*Gai* proteins (Fig. S1). rPtxS1-r*Gai* complex
151 formation during catalysis therefore appears to be weak, i.e. the r*Gai* modification is based on a
152 transient kiss-and-run interaction. Interestingly, rPtxS1 modifies itself (Fig. 2E), and it already
153 had become auto-ADP-ribosylated in the *E. coli* expression host (Fig. 2F). This activity was
154 drastically diminished in a Q127D/E129D double mutant of rPtxS1, hereafter referred to as
155 rPtxS1-mutant (Fig. S2A). The rPtxS1-mutant was also incapable of ADP-ribosylating r*Gai* (Fig.
156 S2B). This double mutant of rPtxS1 was analyzed, because structurally identical mutations in a
157 recently discovered pertussis-like toxin from *E. coli* caused catalytic inactivation, although NAD⁺
158 was still capable of binding to the protein (22)(Fig. S2C). Q127 and E129 of rPtxS1 are also
159 conserved with several other bacterial ART-toxins where these residues position NAD⁺, in
160 particular the nicotinamide end (Fig. S2C), and promote the transfer of ADP-ribose to a substrate
161 amino acid residue (16). To assess the substrate amino acid specificity of the extensively
162 truncated rPtxS1 (see Fig. 1 and Fig. 2A), we analyzed the C351A mutant of r*Gai*
163 (UniProt_P63096), hereafter referred to as r*Gai*-mutant, in an NAD⁺-biotin Western blot-assay.
164 rPtxS1 ADP-ribosylated r*Gai*, but it was incapable of ADP-ribosylating the r*Gai*-mutant (Fig.
165 S3). Based on a DSF-assay, the T_m of the r*Gai*-mutant was 44.33 ± 0.23 °C as compared to T_m

166 of the rGai-wt (T_m of 43.83 ± 0.23 °C), indicating that the C351A mutation does not affect the
167 protein folding. Therefore, rPtxS1 is not only catalytically active towards rGai, but it also retains
168 the Gai substrate amino acid specificity evidenced with the pertussis AB₅ holotoxin (17-19).

169

170 **Multiwell-based assay set-up for screening of rPtxS1 inhibitors** – We analyzed the suitability

171 of a fluorometric method to screen for rPtxS1 inhibitors previously developed for poly-ADP-

172 ribose synthesizing enzymes (23) and later extended to mono-ADP-ribose synthesizing enzymes

173 (24). Briefly, the end point assay is based on conversion of NAD⁺ to a stable fluorophore with

174 emission maximum at 444 nm (23). The decrease in fluorescence in comparison to the non-

175 enzyme control is a measure of NAD⁺-consuming enzymatic activity (23). Incubation of rPtxS1

176 with rGai for 40 min resulted in a strong decrease of fluorescence, almost comparable to the

177 fluorescence signal obtained with the buffer control where no NAD⁺ was added to the reaction

178 (Fig. 3A). No fluorescence decrease was detected with the rPtxS1-mutant under identical

179 conditions (Fig. 3A). Assays with different concentrations of rPtxS1 were stopped at various time

180 points to measure NAD⁺ consumption in the presence of a constant amount of rGai substrate.

181 These data demonstrate that an increase in the rPtxS1 concentration increases NAD⁺

182 consumption that also progresses over time (Fig. 3B). These results indicate that the detected

183 reduction in fluorescence is not an effect of fluorescence quenching but indeed NAD⁺-consuming

184 activity of rPtxS1. rPtxS1 could also consume NAD⁺ in the absence of rGai, although much

185 slower than with the rGai substrate (Fig. 3A). This NAD⁺ glycohydrolase activity, i.e. enzyme-

186 catalyzed reaction between NAD⁺ and water to yield ADP-ribose and nicotinamide, was not

187 detected with the rPtxS1-mutant (Fig. 3A). The effect of DMSO on the NAD⁺-consuming activity

188 of rPtxS1 was also studied because small molecules in chemical libraries are usually dissolved in

189 DMSO typically resulting in assay concentrations of 0.1% – 1% DMSO. DMSO did not have a
190 significant effect on the NAD⁺-consuming activity of rPtxS1 in the presence of rGai substrate up
191 to 0.2% DMSO, while 1% DMSO already significantly ($p = 10^{-4}$) reduced activity (Fig. 3C). We
192 chose to perform screenings in the presence of 0.1% DMSO. To test reproducibility of the
193 fluorometric assay, maximum (NAD⁺ as incubated in plain buffer) and minimum (NAD⁺ as
194 incubated in rPtxS1- and rGai-containing buffer) signals were measured from five independent
195 runs to test plate-to-plate and day-to-day variability. The average Z' value for the assay was 0.68,
196 indicating that the fluorometric assay is suitable for high throughput screening. The statistical
197 parameters of the assay are summarized in Table S1.

198

199 **Screening for rPtxS1 inhibitors** – We screened a chemical library of 1,695 compounds obtained
200 from the National Cancer Institute (NCI) Developmental Therapeutics program repository
201 (<https://dtp.cancer.gov/>). A total of nine compound hits were identified, which inhibited the
202 NAD⁺-consumption activity of rPtxS1 in the presence of rGai more than 50% (screening data not
203 shown). These nine compounds were analyzed in an independent NAD⁺-biotin Western blot-
204 assay, which measures the ADP-ribosylation activity of rPtxS1, i.e. rPtxS1-catalyzed conjugation
205 of ADP-ribose-biotin onto rGai. Five out of the nine primary compound hits showed strong
206 inhibition of the rPtxS1 ADP-ribosylation activity (Fig. 4A). NSC 119875 (Cisplatin, DNA
207 alkylating agent used in cancer treatments) and NSC 44750 affected rGai and/or rPtxS1 protein
208 integrity in the NAD⁺-biotin Western-blot based assay (Fig. 4A), even if the assay was performed
209 with a 10-fold lower compound concentration (data not shown). NSC 119875 and NSC 44750
210 were therefore excluded from further studies. To evaluate the potency of the remaining three
211 compounds for rPtxS1 inhibition, dose response studies were performed using the fluorometric
212 NAD⁺-consumption assay in the presence of rGai. Two of the compounds had an IC₅₀-value of <

213 10 μM with NSC 228155 and NSC 29193 having an IC_{50} -value of 3.0 and 6.8 μM , respectively
214 (Fig. 4B). NSC 149286 was less potent than the other two compounds with an IC_{50} -value of 20
215 μM (Fig. 4B), and was excluded from further analyses. We did not detect NSC 228155- or NSC
216 29193-induced transition of the rPtxS1 sigmoidal melting curves towards higher temperatures in
217 a DSF-assay (Fig. S4). This indicates that either the compound binding is not sufficient to alter
218 the thermal stability of rPtxS1 fold, or that the compound affinity to rPtxS1 is low. Importantly,
219 the transition of the sigmoidal melting curve towards lower temperatures was also not evident,
220 indicating that the compounds do not destabilize rPtxS1. The two hit compounds were not
221 identified as pan-assay interference compounds or aggregators (zinc15.docking.org). In summary,
222 compound library screening resulted into identification of two compounds (NSC 228155 and
223 NSC 29193), which inhibited the rPtxS1-catalyzed ADP-ribosylation of rG α i.

224
225 **Putative binding poses of NSC 29193 and NSC 228155 to PtxS1** – In order to evaluate
226 possible binding modes of the compounds to PtxS1, we performed docking and molecular
227 dynamic simulations (MDS). Docking of NSC 228155 produced multiple binding poses but some
228 features were shared among the top ranked poses, including the placement of the aromatic
229 pyridine ring of NSC 228155 in an enclosed region where the nicotinamide ring of NAD^+ would
230 bind to PtxS1, with the double benzoxadiazole ring positioned near the center of the NAD^+ -
231 binding pocket. The benzoxadiazole ring is joined to the pyridine ring via a central sulfur atom,
232 and the rotatable bonds permit the adoption of varying conformations. In pose 1 (Fig. 5A), with
233 the lowest free energy of binding (ΔG_{bind} of -51.2 kcal/mol; docking score of -4.08 kcal/mol), the
234 pyridine ring oxygen of the ligand forms a hydrogen bond with the main-chain nitrogen atom of
235 Tyr10, anchoring the ligand to an aromatic area of the binding pocket, and with π - π stacking
236 interactions observed for the pyridine ring with nearby Tyr59 and for the benzoxadiazole ring

237 with Tyr63. In pose 2 (Fig. 5B), having the best docking score (-4.20 kcal/mol; ΔG_{bind} of -43.3
238 kcal/mol), the pyridine ring is rotated 90° relative to pose 1, losing the backbone hydrogen bond
239 with Tyr10, but making π - π interactions with both Tyr63 and Tyr10, and ionic interactions with
240 Arg9 and Arg67. In MDS, pose 1 showed stability and retains its position with respect to the
241 original docked position, only differing on average by an RMSD of 0.9 Å (Fig. S5A), and the
242 RMSD for the ligand orientations differ on average by 2.3 Å when the coordinates of PtxS1 are
243 superposed over the backbone atoms. In contrast, pose 2 was very unstable at the initial binding
244 position and occupied different locations of the binding pocket with an average 22 Å RMSD for
245 the ligand based on superposing the PtxS1 coordinates from the simulation (Fig. S5B).

246 In contrast to NSC 228155, NSC 29193 is rigid and almost exclusively resulted in two docked
247 poses. Pose 1 of NSC 29193 is positioned near the binding site for the nicotinamide ring of
248 NAD^+ in the PtxS1, hydrogen bonding with main-chain nitrogen and oxygen atoms of Tyr10
249 (Fig. 5C). Additionally, NSC 29193 forms π -cation interactions with Arg9, π - π stacking with
250 Tyr63 and hydrogen bonding with the side-chain hydroxyl group of Ser52. NSC 29193, pose 2, is
251 bound near the location where the adenine ring of NAD^+ would be bound in the pertussis toxin,
252 stacking against the aromatic ring of Trp26 and hydrogen bonding with the main-chain oxygen
253 atom of Thr24 (Fig. 5D) as well as forming ionic interactions with Arg9 and Arg13. During
254 MDS, NSC 29193 pose 1 was quite stable, with an average RMSD of 0.1 and 1.0 Å with respect
255 to the ligand and receptor backbone atoms (Fig. S5C), and interactions between the ligand and
256 main-chain atoms of Tyr10 were conserved for over 90% of the simulation time. The π - π
257 interactions with Tyr63 and π -cation interactions with Arg9 were also retained for the majority of
258 the simulation time. In contrast, the binding mode of pose 2 was disrupted at around 20 ns of the
259 simulation (Fig. S5D), mainly due to the reorientation of the indole ring of Trp26, which appears
260 to be one of the key interaction partners of NSC 29193. Consequently, in pose 2 the ligand moves

261 from the initial binding position and binds to several areas of the binding pocket. This is reflected
262 by the average 12 Å RMSD of the ligand with respect to the superposed coordinates of the toxin
263 from the simulation (Fig. S5D). Taken together, docking and MDS resulted in identification of
264 plausible binding poses of NSC 228155 and in particular for NSC 29193, most likely owing to
265 the rigidity of the latter ligand, at the NAD⁺-binding pocket of PtxS1.

266

267 **Inhibitory action of NSC 228155 and NSC 29193 in a living human cell-based assay** – First,
268 to find the optimal toxin dosage, we titrated the pertussis AB₅ holotoxin and detected the ADP-
269 ribosylation of endogenous G α i by Western blot-assay using a polyclonal mono-ADP-ribose-
270 recognizing antibody. Incubation of cells for 2 h with the holotoxin resulted, in a concentration
271 dependent-manner, mono-ADP-ribosylation of a single protein migrating between the 35 and 55
272 kDa protein markers in SDS-PAGE (Fig. 6A), in accordance with a theoretical size of
273 endogenous G α i, e.g. 40.4 kDa for isoform 1 (UniProt_P63096). Next, we pre-incubated the cells
274 with the compounds NSC 228155 or NSC 29193 prior to addition of the holotoxin and
275 subsequent co-incubation. We did not detect any inhibitory action for the compound NSC 29193
276 despite multiple analyzed conditions (data not shown), e.g. i) 30 min pre-incubation with
277 inhibitor (0.1, 1, 10 and 50 μ M) + 2 h with holotoxin (10 ng/mL) or ii) 1, 2, 3, 4 and 5 h pre-
278 incubation with 50 μ M inhibitor + 2 h with holotoxin (10 ng/mL). However, compound NSC
279 228155 inhibited the G α i-specific ADP-ribosylation activity of holotoxin in a concentration-
280 dependent manner (Fig. 6B). Pre-incubation of the cells for 30 min with 5 μ M of NSC 228155
281 prior to holotoxin addition and subsequent co-incubation resulted in a near complete inhibition of
282 mono-ADP-ribosylation of G α i (Fig. 6B). Importantly, NSC 228155 inhibited the holotoxin
283 activity in concentrations that were not deleterious for the cell viability. First of all, we did not
284 detect major visual alterations in HEK293T monolayers upon 5 μ M NSC 228155 incubation

285 during the 2.5 h *in vivo* ADP-ribosylation assay period (data not shown). Secondly, cell viability,
286 as analyzed by the MTT-assay at 3.5 h after addition of NSC 21855, was significantly affected
287 only after 20 μ M or higher concentration was used (Fig. S6A). IC₅₀ of the NSC 228155
288 cytotoxicity in HEK293T was 15.33 μ M (Fig. S6A). Thirdly, 5 μ M NSC 228155 did not
289 significantly increase the DNA-damage induced PARP1 (also called ARTD1) poly-ADP-
290 ribosylation or cell death-associated PARP1/ARTD1 proteolytic processing from the
291 approximately 120 kDa full length form into approximately 90 kDa form (Fig. S6B). Taken
292 together, compound NSC 228155 inhibits the AB₅ holotoxin-catalyzed ADP-ribosylation of Gai
293 in living HEK293T cells in concentrations that are not deleterious for the cell viability.

294

295 **DISCUSSION**

296 We report the identification of the first small molecular weight compounds inhibiting the ADP-
297 ribosyltransferase activity of pertussis toxin *in vitro* and in living cells. Compound library
298 screening was made possible due to our ability to purify mg-levels of a truncated but highly
299 active recombinant PtxS1 (rPtxS1) under native conditions from *E. coli*. Moreover, rPtxS1
300 retained the high amino acid specificity of pertussis AB₅ holotoxin toward the single C-terminal
301 cysteine in Gai (17-19). Used truncation positions in rPtxS1 are functionally justified. PtxS1
302 contains an N-terminal signal sequence ending at Ala34 (25, 26) that gets cleaved upon the Sec-
303 mediated secretion of PtxS1 from the cytoplasm into the periplasm where the AB₅ holotoxin is
304 assembled prior to Ptl type IV secretion system-mediated export. Asp35 is classically numbered
305 as the first amino acid of mature PtxS1 (see Fig. 2). The truncated part of the PtxS1 C-terminus
306 (see Fig. 1, 2A) masks the NAD⁺-binding pocket in the AB₅ holotoxin involving a stabilizing
307 intramolecular di-sulfide bond between Cys41 and Cys201 (12, 13). Our truncation approach
308 bypasses the need for disulfide bond reduction (27) and extensive conformational movement of

309 the C-terminus (12, 13) to activate PtxS1, which inside the host cell has also been proposed to
310 involve proteolysis (28).

311 The inhibitory compounds NSC 29193 and NSC 228155 with low micromolar IC₅₀-values
312 were identified in the *in vitro* NAD⁺ consumption assay from a chemical library of 1,695
313 compounds. These compounds were also potent in an independent *in vitro* assay where we
314 monitored the amount of rGai-conjugated ADP-ribose-biotin upon rPtxS1 catalysis by
315 streptavidin-HRP Western blotting (see Fig. 4A). It is noteworthy that other compounds were
316 also positive in the *in vitro* NAD⁺ consumption assay, but apparently via deleterious effects for
317 protein stability as evidenced by the independent *in vitro* ADP-ribose conjugation assay, i.e.
318 compounds NSC 44750 and NSC 119875 (cisplatin) (see Fig. 4A). We did not detect NSC
319 228155- or NSC 29193-induced transition of the rPtxS1 sigmoidal melting curves towards higher
320 temperatures in a DSF-assay (see Fig. S4). This indicates that either the compound binding is not
321 sufficient to alter the thermal stability of rPtxS1 fold, or the affinity of the compounds to rPtxS1
322 is low. With respect to NSC 228155, we also attempted to utilize its inherent fluorescence (29) in
323 a fluorescence polarization assay, but we did not detect significant changes in fluorescence
324 polarization to make reliable conclusions on the affinity of NSC 228155-rPtxS1 interaction (data
325 not shown). Our docking and molecular dynamic simulations resulted in variability among poses
326 for both ligands. More consistent, energetically favorable binding poses were observed for NSC
327 29193. This is in accordance with the compound structures (see Fig. 4C). NSC 29193 (purine-
328 2,8-dithiol) is a rather rigid purine analogue that mimics the structure of the adenine base of
329 NAD⁺. NSC 228155, on the other hand, contains two major molecular structures, connected by a
330 rotatable linker, one ring compound mimicking the adenine base of NAD⁺ and the other ring
331 compound mimicking the nicotinamide of NAD⁺. In summary, compound library screening

332 resulted into the identification of two compounds, NSC 29193 and NSC 228155, which inhibited
333 the rPtxS1-catalyzed ADP-ribosylation of rGai *in vitro*.

334 NSC 228155, but not NSC 29193, was a potent inhibitor of pertussis holotoxin-mediated
335 ADP-ribosylation of Gai in living HEK293T cells. We tried multiple different experimental set-
336 ups with NSC 29193 (see Results section, last chapter), including concentrations as high as 50
337 μM that still did not cause visible alterations for HEK293T cell monolayers. In respect of
338 previous drug screening approaches there appears to be little if any published information on
339 NSC 29193. The cell permeability of NSC 29193 is not known, but might be weak and thus
340 explain our negative inhibitory data. In sharp contrast, we detected a near complete inhibition of
341 the ADP-ribosylation with 5 μM NSC 228155 (see Fig. 6). In part, this could relate to the fact
342 that NSC 228155 easily permeates cells. It has been shown in MDA-MB-468 breast cancer cells
343 that 5 min incubation with 100 μM NSC 228155 caused rapid movement of this inherently
344 fluorescent molecule across cell membranes and dispersal to both the cytoplasm and nucleus
345 (29). However, we witnessed significant toxicity of NSC 228155 for HEK293T cells with 20 μM
346 or higher concentrations after a 3.5-h incubation (cytotoxicity IC_{50} – 15.33 μM). This cytotoxicity
347 might be caused by the proposed NSC 228155-mediated production of reactive oxygen species
348 (ROS) inside the cell (29). In this respect, it is noteworthy that, upon incubation of cells with 5
349 μM of NSC 228155 for 2.5 h, we did not detect auto-ADP-ribosylation of PARP1/ARTD1 (see
350 Fig. S6), which is induced in cells upon ROS-induced DNA damage (30). Moreover, we did not
351 detect caspase-mediated proteolytic PARP1/ARTD1 cleavage (see Fig. S6), which is a robust
352 readout for the onset of programmed cell death. However, future lead development needs to
353 address the apparent cell toxicity effects of NCS 228155. Taken together, NSC 228155 is a cell
354 permeable and potent compound to inhibit pertussis holotoxin-mediated ADP-ribosylation of Gai
355 in living cells in low micromolar concentration.

356 Resurgence of pertussis has been witnessed even in highly vaccinated populations (1-3), and
357 there are no specific therapeutics to treat whooping cough. Macrolide antibiotics, when
358 administrated at a very early stage, show therapeutic effects in certain patient subgroups such as
359 in infants <3 months of age (31). However, macrolide resistant *B. pertussis* strains have been
360 reported (32, 33). Pertussis toxin is a major virulence factor of *B. pertussis*, and appears to
361 contribute to the development of whooping cough (6-11). Targeting of pertussis toxin might
362 prove beneficial in the treatment of whooping cough, especially in young children who still lack
363 the vaccine-induced protection against pertussis. In this respect, several drug modes of action
364 could be envisioned, including to inhibit – i) secretion, ii) host cell recognition, iii) endocytosis,
365 iv) intracellular trafficking, and v) enzymatic activity (i.e. ADP-ribosylation) inside the host cell.
366 Humanized monoclonal antibodies have been developed that block pertussis toxin cell surface
367 receptor interaction or the subsequent internalization and retrograde trafficking (34). These
368 humanized antibodies prevented the characteristic signs of pertussis in mouse and baboon models
369 (35). Our current study shows that small molecular weight compounds inhibiting the ADP-
370 ribosyltransferase activity of pertussis toxin might also have therapeutic potential. Similar
371 findings have been published on other ADP-ribosylating bacterial toxins, such as ExoA and ExoS
372 of *Pseudomonas aeruginosa* and cholix-toxin of *Vibrio cholerae* (36, 37). We conclude that NSC
373 29193 and NSC 228155 are useful templates for future lead development to specifically inhibit
374 pertussis toxin activity, the immediate challenge being to enhance target specificity and to
375 increase affinity.

376

377

378

379

380 MATERIALS AND METHODS

381 **Expression plasmids – i) *rPtxS1-wt*** Synthetic DNA fragment (Eurofins Genomics) encoding for
382 amino acids D35-I221 of *Bordetella pertussis* strain Tohama I (UniProt_P04977) was cloned
383 with NdeI and BamHI into pET15b (Novagen) allowing expression of an N-terminally HIS-
384 tagged rPtxS1 (MGSSHHHHHHSSGLVPRGSHM-D35-PtxS1-I221). The D35-I221 truncation
385 positions of PtxS1 are based on (38). Of note, Asp35 is classically numbered as the first amino
386 acid of PtxS1. **ii) *rPtxS1-Q161D/E163D*** pET15b-rPtxS1 plasmid was linearized with PCR using
387 5'-phosphorylated oligonucleotide primers (Eurofins Genomics) prAPV-351
388 (GATAGCGATTATCTGGCACACCGGCGCATTCCG, mutagenic nucleotides underlined) and
389 prAPV-352 (GTAGGTGGCCAGCGCGCCGGCGAGGATACG). The PCR product was gel-
390 isolated, re-ligated and transformed to acquire the mutant plasmid. **iii) *rGai-wt*** Synthetic DNA
391 fragment (GenScript) encoding for *E. coli* codon-optimized full-length human Gai (isoform 1,
392 UniProt_P63096-1) was cloned into pNIC-Bsa4 (Structural Genomics Consortium) using the
393 ligation independent cloning method allowing expression of an N-terminally HIS-tagged rGai
394 (MHHHHHHSSGVLDLGTENLYFQS-Gai). **iii) *rGai-Cys351Ala*** rGai-encoding plasmid was
395 used as a template in PCR to amplify Cys351Ala-mutant-encoding mutant allele using
396 oligonucleotide primers (Eurofins Genomics) prAPV-418
397 (tacttccaatccATGGGTTGCACCCTGAGCGCGGAA, LIC-cloning overhangs in lowercase) and
398 prAPV-419 (tatccaccttactgTCAGAACAGGCCCGCATCCTTCAGGTTGTTCTTG, mutagenic
399 nucleotides underlined, LIC-cloning overhangs in lowercase). The PCR product was cloned into
400 pNIC-Bsa4 (Structural Genomics Consortium) using the ligation independent cloning method
401 allowing expression of an N-terminally HIS-tagged rGai-Cys351Ala mutant similar to rGai-wt.
402 All expression plasmids were verified by sequencing.

403

404 **Protein expression and purification** – Expression plasmids were transformed into BL21(DE3)
405 (Novagen) and selected overnight at 37°C on Luria-Bertani (LB) agar with appropriate
406 antibiotics. Next morning, the bacterial lawn from the LB-plates was transferred into Terrific
407 broth autoinduction medium (Formedium, AIMTB0205) supplemented with 0.8% (w/v) of
408 glycerol with appropriate antibiotics. Cultures were grown at 37°C with 250 rpm until optical
409 density at 600 nm reached 1 (typically 3-5 h), and temperature was reduced to 18°C. Bacteria
410 were collected after 24 h by centrifugation and were either frozen to -80°C as pellets, in lysis
411 buffer or directly used for purification. Pefabloc protease inhibitor (Roche, 11585916001) was
412 added to 0.1 mM in the thawed biomass in lysis buffer [100 mM Hepes (pH 7.5), 500 mM NaCl,
413 10% (w/v) glycerol, 0.5 mM Tris(2-carboxyethyl)phosphine hydrochloride (TCEP), 10 mM
414 imidazole]. Samples were sonicated and clarified by centrifugation. Supernatant was loaded to 5
415 mL HisTrap HP column (GE Healthcare). With rPtxS1 proteins, column was washed with 10
416 column volumes of wash buffer I and II. Wash buffer I and II have identical compositions to lysis
417 buffer with the exception of imidazole concentration of 25 and 50 mM, respectively. rPtxS1
418 proteins were eluted with elution buffer [100mM Hepes (pH 7.5), 500 mM NaCl, 10% (w/v)
419 glycerol, 0.5 mM TCEP, 500 mM imidazole], concentrated using a 10 kDa cut-off concentrator
420 (Thermo Scientific) and subjected to size exclusion chromatography on Superdex75 16/600
421 Hiload Superdex column (GE Healthcare) using SEC buffer [100 mM Hepes (pH 7.5), 500 mM
422 NaCl, 10% (w/v) glycerol, 0.5 mM TCEP]. With Gai proteins, HisTrap HP column was washed
423 with 15 column volumes of wash buffer [20mM Hepes (pH 7.5), 500 mM NaCl, 10% (w/v)
424 glycerol, 0.5 mM TCEP, 25 mM imidazole] and eluted with elution buffer [20 mM Hepes (pH
425 7.5), 500 mM NaCl, 10% (w/v) glycerol, 0.5 mM TCEP, 500 mM imidazole]. Fractions were
426 concentrated using a 10 kDa cut-off concentrator (Thermo Scientific) and further purified by size

427 exclusion chromatography on Superdex75 16/600 Hiload Superdex column (GE Healthcare) with
428 SEC buffer [30 mM Hepes (pH 7.5), 350 mM NaCl, 1 mM MgCl₂, 0.5 mM TCEP]. Protein
429 fractions were pooled, concentrated using a 10 kDa cut-off concentrator (Thermo Scientific),
430 flash frozen and stored in -80°C.

431

432 **Static light scattering** – All experiments were conducted with SEC-MALS buffer [100 mM
433 Hepes (pH 7.5), 500 mM NaCl, 10% (w/v) glycerol, 0.5 mM TCEP] with a flow rate of 0.150 mL
434 per minute. Buffer was filtered with 0.1 µm filter to remove small particles. Typically 100 µg of
435 protein samples were injected into Superdex 200 10/300 increase column (GE Healthcare) by a
436 Shimadzu autosampler coupled HPLC machine. Light scattering data were recorded using a
437 multiangle light scattering detector (miniDAWN TREOS, Wyatt technology). Data were
438 analyzed using Astra software (Wyatt technology). For complex formation studies, 1:1 molar
439 ratio of rPtxS1 and rGαi (100 µg in total) was incubated on ice for 2 h and then injected into the
440 column.

441

442 **Differential scanning fluorimetry (DSF)** – rPtxS1 at a concentration of 0.25 mg/mL was used
443 in PBS. Protein was incubated with 5 × SYPRO orange (Thermo Scientific) for 10 minutes. The
444 samples were heated from 20-90°C with 1°C increments (1 min/1°C). The experiment was run on
445 2500 Real-Time PCR systems (Applied Biosystems). The resulting data was analyzed with
446 Boltzmann sigmoidal equation using GraphPad (GraphPad software, Inc.). Thermal stability of
447 rGαi, rGαi-mutant and rPtxS1 alone as well as in the presence of NSC 228155 or NSC 29193,
448 was analyzed by DSF using a CFX96 Real-Time PCR detection system (Bio-Rad). rGαi, rGαi-
449 mutant and rPtxS1 at a concentration of 0.2 mg/mL was used in 20 mM Hepes (pH 7.5), 500 mM

450 NaCl, 10% (w/v) glycerol, 0.5 mM TCEP. The inhibitor concentrations used in the assay ranged
451 from 50 μ M to 1 mM. Samples were incubated with 5 \times SYPRO Orange (Thermo Scientific) for
452 5 min. The samples were heated from 20-90°C with 0.5°C increments (1 min/1°C). T_m-values
453 were determined by using the CFX96 Real-Time PCR detection system (Bio-Rad) software.

454
455 ***In vitro* ADP-ribosylation assays – i) enzyme-excess condition** Reactions (typically in 120 μ L)
456 contained 10 μ M rPtxS1 proteins, 10 μ M biotinylated NAD⁺ (Trevigen, 4670-500-01) or 10 μ M
457 NAD⁺ (Sigma, N3014) and either 4 μ M rGai proteins or membrane fraction of HEK293T cells
458 (30 μ g of total protein) as the substrate in 100 mM Hepes (pH 7.5), 500 mM NaCl and 10% (w/v)
459 glycerol. The membrane fraction was prepared essentially as described in (39). 80% confluent 10
460 cm cell culture plate of HEK293T cells was placed on ice and washed twice with PBS. Cells
461 were collected by scraping into 1 mL of hypotonic lysis buffer [20 mM Hepes (pH 7.5), 2.5 mM
462 MgCl₂, 1 mM DTT supplemented with Pierce Protease and Phosphatase Inhibitor Mini Tablets
463 (40 μ L/mL of stock solution – one tablet / 2 mL H₂O, Thermo Scientific, 88668) and 25 U/mL of
464 benzonase (Merck-Millipore, 70664-3)]. The cells were incubated at 4°C for 1 h in rotation to
465 allow them to swell and partially lyse. The partial lysates were drawn 20 times through 27-gauge
466 needles and centrifuged with low speed (600 \times g, 4°C, 10 min) to pellet the nuclei and insoluble
467 cell debris. The low-speed supernatant was subjected to high-speed centrifugation (16100 \times g,
468 4°C, 30 min) to pellet the membranes. The membranes were resolubilized into 50 μ L of 50 mM
469 Hepes (pH 7.5), 200 mM NaCl, 1 mM EDTA and 10 mM DTT, 0.3% (w/v) SDS and 2% Triton
470 X-100 supplemented with protease and phosphatase inhibitors, in concentration as described
471 above. Protein concentration was measured with Bradford assay. The ADP-ribosylation reactions
472 were carried out at room temperature for 3 h with shaking at 300 rpm. Reactions were stopped by

473 addition of Laemmli loading dye to 1 × and heating for 10 minutes at 95°C. The samples were
474 run on SDS-PAGE and transferred to nitrocellulose membranes, followed by blocking with 1%
475 (w/v) casein blocking buffer (Bio-Rad, 161-0782). Membranes were incubated with streptavidin
476 conjugated to horse radish peroxidase (1:5000) (GE Healthcare, RPN1231VS) in 1% (w/v) casein
477 blocking buffer (Bio-Rad, 161-0782) for 3 h at 4°C in rotation and washed thrice with Tris-
478 buffered saline [10 mM Tris-HCl (pH 7.5), 150 mM NaCl] containing 0.05% Tween 20 (TBST)
479 for ten minutes each time. Alternatively, after blocking with 4% (w/v) BSA in TBST, membranes
480 were probed in TBST containing 2% (w/v) BSA (24 - 48 h at 4°C in rotation) for HIS-tagged
481 rPtxS1 and rGai proteins with mouse monoclonal anti-HIS (1:1000) (R&D Systems, MAB050),
482 for Gai with mouse monoclonal anti-Gai (1:500) (Santa Cruz Biotechnology, sc-136478) or
483 mono-ADP-ribose with a rabbit polyclonal anti-mono-ADP-ribose (1:1000) antibody (Hottiger-
484 laboratory). Primary antibody membranes were washed thrice with TBST containing 2% (w/v)
485 BSA for ten minutes each time. Primary antibody membranes were incubated with mouse IgG
486 kappa binding protein conjugated to horseradish peroxidase (1:2500) (sc-516102, Santa Cruz
487 Biotechnology) or goat anti-rabbit IgG conjugated to horseradish peroxidase (1:2500) (sc-2004,
488 Santa Cruz Biotechnology) for 3 h at 4°C in rotation and washed thrice with TBST for ten
489 minutes each time. All membranes were subsequently developed with WesternBright ECL
490 (Advansta) and imaged on ImageQuant LAS 4000 (GE Healthcare). **ii) substrate-excess**
491 **condition** Reactions (typically in 50 µL) contained 50 nM PtxS1 proteins and 500 nM Gai in 50
492 mM sodium phosphate (pH 7.0) and 1 µM biotinylated NAD⁺ (Trevigen, 4670-500-01). The
493 reactions were carried at room temperature for 40 minutes. For validating hits from chemical
494 screening, 10 µM of the indicated compound and 0.1% DMSO (control reaction) were used.
495 Reactions were stopped by addition of Laemmli loading dye to 1 × and heating for 3 minutes at

496 90°C. The samples were run on SDS-PAGE and transferred to nitrocellulose membranes,
497 followed by blocking with 1% (w/v) casein blocking buffer (Bio-Rad, 161-0782). Membranes
498 were incubated with streptavidin conjugated to horse radish peroxidase (1:7000) (PerkinElmer,
499 NEL750001EA) in 1% (w/v) casein blocking buffer (Bio-Rad, 161-0782) for 3 h at 4°C in
500 rotation and washed thrice with TBST for ten minutes each time. Alternatively, for anti-His
501 blotting, Penta His HRP conjugate (Qiagen, 34460) was diluted 1:5000 in 1% (w/v) casein
502 blocking buffer (Bio-Rad, 161-0782). Blots were incubated at room temperature for 2 h, followed
503 by 3 washes with TBST each for 5 minutes. Membranes were subsequently developed with
504 WesternBright ECL (Advansta) and imaged on ChemiDoc XRS+ (Bio-Rad).

505
506 ***In vitro* NAD⁺ consumption assay – i) basic reaction set-up** Reactions were carried out in a U-
507 shaped 96-well black plate (Greiner BioOne, 650209). Typically, reactions were conducted with
508 50 mM sodium phosphate (pH 7.0) at 25°C with shaking at 300 rpm with a reaction volume of 50
509 µL. The reactions were stopped by adding 20 µL of 20% acetophenone (diluted with ethanol) and
510 20 µL of 2M KOH and incubated at room temperature for 10 minutes. 90 µL of formic acid was
511 added and further incubated for 20 minutes. The plates were read using Tecan infinity M1000 pro
512 with excitation and emission wavelengths set at 372 and 444 nm, respectively. Maximum signal
513 was defined as the NAD⁺ buffer control and the minimum signal was the rPtxS1-catalyzed
514 reaction in the presence of rGai. The raw fluorescence values were always subtracted from blank
515 containing buffer. The assay was optimized to reach 60% NAD⁺ consumption. The optimized
516 conditions for the assay are 125 nM rPtxS1, 500 nM NAD⁺ and 1 µM rGai. The reaction has
517 incubation time of 40 minutes at 25°C with shaking at 300 rpm. The DMSO concentration used
518 was 0.1%. DMSO tolerance test was done with optimized conditions (0.1-5%). For rGai
519 substrate-independent NAD⁺ consumption activity of rPtxS1, identical conditions were used

520 except that rGai was excluded with longer incubation time of 60 minutes. Statistical analyses on
521 typically 8 parallel values was conducted using two-tailed Student's t-test two sample equal
522 variance (homoscedastic). **ii) validation of the NAD⁺ consumption assay** In order to establish
523 repeatability of values for maximum and minimum signals between plates, wells and days, five
524 control plates were tested. Experimental conditions and protein batches used for assay validation
525 were the same. Three plates were made on one day while second and third days had one plate
526 each. Each plate had 40 wells for maximum and minimum signals individually with buffer
527 blanks. The CV% were calculated separately for minimum and maximum signals using (Standard
528 deviation/average) *100. Assay parameters such as signal-to-noise (S/N), (S/B) signal-to-
529 background, screening window coefficient (Z') were calculated as described previously (23, 24).
530 **iii) small molecule library screening** Each plate had buffer blank, control reaction (minimum
531 signal, with rPtxS1-wt) and maximum signal (NAD⁺ and rGai). Both maximum and minimum
532 signals contain 0.1% DMSO. To correct for inherent fluorescence of compounds separate
533 controls with NAD⁺, Gai and compounds were prepared. Compounds were tested at a
534 concentration of 10 μ M. Compounds displaying inhibition more than 50% were considered as
535 hits. Compound libraries for chemical screening were obtained from NCI repository. **iv) IC₅₀**
536 **measurements** Assay incubation time was adjusted such that the substrate conversion did not
537 exceed 30% in order to minimize the effect of reduction in substrate concentration while
538 maintaining a robust signal. Compounds were tested from a concentration range of (100-0.01
539 μ M) in half-log dilution series. Each plate had buffer blank, positive control where PtxS1-wt is
540 added which corresponds to 100% activity and negative control (without enzyme) where the
541 activity was 0%. Control values were included as two half-log units below and above the
542 inhibitor concentration series for reactions with 0% and 100% activity. IC₅₀ values were obtained
543 by fitting data to log (inhibitor) vs response - variable slope using GraphPad (GraphPad software,

544 Inc.) Chemical structures were drawn using MarvinSketch 5.11.3 (chemAxon) or ChemDraw
545 18.0 (Perkin-Elmer).

546

547 **Structure preparation and molecular docking** – The 2.7 Å resolution crystal structure of
548 pertussis toxin was accessed from the Protein Data Bank (PDB) (PDB_1BCP (15)). Herein, we
549 considered only the catalytic PtxS1 subunit (1BCP, chain A). Residues 222-269 of PtxS1 were
550 also removed from the coordinate file (see Fig. 1 and 2). The truncated structure was then
551 prepared for docking using the protein preparation wizard (40) in Maestro (Schrödinger Release
552 2019-1: Maestro, Schrödinger, LLC, New York, NY, 2019). Hydrogen atoms were added,
553 protonation states of ionizable groups were determined and the structure was energy minimized.
554 A grid outlining the binding pocket was specified based on the superimposition of the PtxS1
555 structure with the S1 subunit of the pertussis-like toxin structure from *E. coli* with bound NAD⁺
556 (PDB_4Z9D; (22)). The two toxins are 30% identical in primary amino acid sequence. The
557 ligands NSC 228155 (7-nitro-4-(1-oxidopyridin-1-ium-2-yl)sulfanyl-2,1,3-benzoxadiazole) and
558 NSC 29193 (purine-2,8-dithiol) were prepared for docking using the LigPrep program in Maestro
559 (Schrödinger Release 2019-1: LigPrep, Schrödinger, LLC, New York, NY, 2019). Possible
560 ionization states of the ligands at pH 7.0 ± 2.0 were determined and, in the case of NSC 29193,
561 four tautomeric states were also produced. The ligands were docked to the pertussis S1 structure
562 using the glide XP and SP methods (41), keeping the protein structure rigid but allowing ligand
563 flexibility, producing up to 20 poses for each ligand and tautomer. Since the resulting XP docking
564 poses exhibited few interactions, the SP docking results were pursued further. The poses were
565 ranked according to the glide docking score and free energy of binding calculations made with

566 the Prime MM-GBSA module (Schrödinger Release 2019-1: Prime, Schrödinger, LLC, New
567 York, NY, 2019).

568

569 **Molecular dynamics simulation** – Molecular dynamics simulation (MDS) of the selected
570 binding poses of NSC 228155 and NSC 29193 bound to the S1 structure was used to study the
571 dynamics of the protein-ligand complexes using the Desmond program (42) in Maestro. The
572 complexes were solvated using a TIP3P water model (43) in an octahedral box, with a 10 Å
573 distance between solute surface atoms and an edge of the box. The systems were neutralized by
574 adding Na⁺ counterions. Additional Na⁺/Cl⁻ ions were added to bring the systems to a 150 mM
575 salt concentration. The simulations were carried out using the OPLS3e force field (44) at constant
576 temperature (300 K) and constant pressure (1 atm), which were respectively regulated using the
577 Nose-Hoover chain thermostat (45) and Martyna-Tobias-Klein barostat (46). Short-range and
578 long-range interactions were computed with a 9 Å distance cutoff. The RESPA integrator (47)
579 was employed with a 6.0 fs time step for long-range non-bonded interactions and a 2.0 fs time
580 step for bonded and short range non-bonded interactions. The systems were relaxed with the
581 default equilibration protocol in Desmond, followed by a 100 ns production simulation. Energies
582 were saved every 1.2 ps, whereas coordinates were recorded every 100 ps. The resulting
583 trajectories were analyzed in terms of ligand stability (as root mean squared deviation, RMSD)
584 and lifetime of protein-ligand interactions using the Simulation Interactions Diagram application
585 in Desmond.

586

587 ***In vivo* ADP-ribosylation assay** – HEK293T cells grown in DMEM + 10% FBS were seeded in
588 3 mL volumes in 6-well plates (500 000 cells/well) in the late afternoon. The next morning fresh
589 media containing NSC 228155 at concentrations of 0.1, 1 and 5 μM was exchanged to the cells

590 (0.05% DMSO in all reactions, including control reactions). Cells were incubated for 30 minutes
591 at 37°C under normal cell culturing conditions, after which 10 ng/mL of pertussis AB₅ holotoxin
592 (List Biological Laboratories Inc., 179A) was added to the cells and incubation was continued for
593 2 h. Cells were then transferred on ice and washed twice with 1 × PBS and collected into 70 µL
594 of lysis buffer [50 mM Tris-HCl (pH 7.5), 400 mM NaCl, 0.1% sodium deoxycholate, 1% NP-40,
595 75 µM tannic acid (PARG inhibitor), 40 µM PJ34 (PARP inhibitor) supplemented with Pierce
596 Protease and Phosphatase Inhibitor Mini Tablets (40 µL/mL of stock solution – one tablet / 2 mL
597 H₂O, Thermo Scientific, 88668). Samples were kept on ice for 30 minutes and centrifuged for 15
598 minutes, 4°C, 16100 × g. Protein concentration was measured from the supernatants with
599 Bradford protein assay. The samples were scaled for protein content to allow loading of 30 µg of
600 total protein per lane in the SDS-PAGE. Laemmli loading dye was added to 1 × and the samples
601 were boiled for 10 minutes at 95°C. The samples were run on SDS-PAGE and transferred to
602 nitrocellulose membranes, followed by blocking with 4% (w/v) BSA in TBST. Membranes were
603 probed in TBST containing 2% (w/v) BSA for mono-ADP-ribose with custom in-house rabbit
604 polyclonal anti-mono-ADP-ribose (1:1000) (Hottiger-laboratory), for GAPDH with mouse
605 monoclonal anti-GAPDH (1:1000) (Abcam, ab9484), for Gai with mouse monoclonal anti-Gai
606 (1:500) (Santa Cruz Biotechnology, sc-136478), for poly-ADP-ribose with rabbit polyclonal anti-
607 PAR (1:1000) (Enzo Life Sciences, ALX-210-890A) and for PARP1 with mouse monoclonal
608 anti-PARP1 (1:300) (Santa Cruz Biotechnology, sc-8007). Membranes were washed thrice with
609 TBST containing 2% (w/v) BSA for ten minutes each time. Membranes were incubated in TBST
610 containing 2% (w/v) BSA with mouse IgG kappa binding protein conjugated to horseradish
611 peroxidase (1:5000) (sc-516102, Santa Cruz Biotechnology) or goat anti-rabbit IgG conjugated to
612 horseradish peroxidase (1:5000) (sc-2004, Santa Cruz Biotechnology) for 3 h at 4°C on a rotary

613 and washed thrice with TBST for ten minutes each time. Membranes were subsequently
614 developed with WesternBright ECL (Advansta) and imaged on ImageQuant LAS 4000 (GE
615 Healthcare).

616
617 **MTT cell viability assay** – HEK293T cells grown in DMEM + 10% FBS were seeded in 100 μ L
618 volumes in 96-well plates (20 000 cells/well) in the late afternoon. The next morning fresh media
619 containing varying concentrations (0, 0.1, 0.5, 1, 2.5, 5, 10, 20, 40, 60 μ M) of NSC 228155 was
620 added in triplicate. In all the wells final concentration of DMSO was 0.6%. Cells were incubated
621 for 2.5 h at 37°C under normal cell culturing conditions. Cell viability was investigated using the
622 CellTiter 96 Non-Radioactive Cell Proliferation Assay (MTT) (Promega, G4002) according to
623 the manufacturer's instructions. Incubation time with the MTT dye solution was 1 h at 37°C
624 under normal cell culturing conditions. NSC 228155 cytotoxicity IC₅₀ value was calculated using
625 GraphPad (GraphPad software, Inc.) Data are displayed as means and the standard error of the
626 mean. Data were normalized to cells treated with 0.6% DMSO (negative controls, 100%
627 viability) and cells killed with 200 μ M H₂O₂ (positive control, 0% viability) and expressed as
628 percentage of these controls. Normalized response is compared to common log of the inhibitor
629 concentration (μ M) and the IC₅₀ calculated using a variable slope. Statistical analyses were
630 conducted using two-tailed Student's t-test two sample equal variance (homoscedastic).

631

632

633

634

635

636

637 **ACKNOWLEDGMENTS**

638 The research in the laboratory of A.T.P. is financially supported by Academy of Finland (grant
639 no. 295296), Sigrid Jusélius Foundation, Turku Doctoral Programme of Molecular Medicine
640 (TuDMM) (to M.M.) and University of Turku, Turku, Finland. This work was funded in the L.L.
641 laboratory by Academy of Finland (grant no. 287063, 294085 and 319299). The use of the
642 facilities of the Biocenter Oulu for DNA sequencing, Proteomics and Protein Analysis and
643 Protein Crystallography, a member of Biocenter Finland and Instruct-FI, are gratefully
644 acknowledged. The laboratory of M.S.J. is supported by Sigrid Jusélius Foundation, Joe, Pentti
645 and Tor Memorial Fund, and Doctoral Network of Informational and Structural Biology (to M.T.,
646 Åbo Akademi Graduate School); computational infrastructure and core faculty support from
647 Biocenter Finland (bioinformatics, structural biology and drug discovery and chemical biology
648 nodes), CSC IT Center for Science; Academy of Finland FIRI infrastructure funding (grant no.
649 320005); screening core faculty of Biocity Turku, and Drug Discovery and Diagnostics strategic
650 funding to Åbo Akademi University. We thank Dr. Jukka Lehtonen for his scientific IT support.
651 The funders had no role in study design, data collection and interpretation, or the decision to
652 submit the work for publication. The authors declare that they have no conflicts of interest.

653

654

655

656

657

658

659

660

661 **REFERENCES**

- 662 1. Kilgore PE, Salim AM, Zervos MJ, Schmitt HJ. 2016. Pertussis: microbiology, disease,
663 treatment, and prevention. *Clin Microbiol Rev* 29:449-86.
- 664 2. Yeung KHT, Duclos P, Nelson EAS, Hutubessy RCW. 2017. An update of the global
665 burden of pertussis in children younger than 5 years: a modelling study. *Lancet Infect Dis*
666 17:974-980.
- 667 3. Skoff TH, Baumbach J, Cieslak PR. 2015. Tracking pertussis and evaluating control
668 measures through enhanced pertussis surveillance, Emerging Infections Program, United
669 States. *Emerg Infect Dis* 21:1568-73.
- 670 4. Thierry-Carstensen B, Dalby T, Stevner MA, Robbins JB, Schneerson R, Trollfors B. 2013.
671 Experience with monocomponent acellular pertussis combination vaccines for infants,
672 children, adolescents and adults - a review of safety, immunogenicity, efficacy and
673 effectiveness studies and 15 years of field experience. *Vaccine* 31:5178-91.
- 674 5. Bouchez V, Brun D, Cantinelli T, Dore G, Njamkepo E, Guiso N. 2009. First report and
675 detailed characterization of *B. pertussis* isolates not expressing Pertussis Toxin or Pertactin.
676 *Vaccine* 27:6034-41.
- 677 6. Carbonetti NH. 2015. Contribution of pertussis toxin to the pathogenesis of pertussis
678 disease. *Pathog Dis* 73:ftv073.
- 679 7. Melvin JA, Scheller EV, Miller JF, Cotter PA. 2014. *Bordetella pertussis* pathogenesis:
680 current and future challenges. *Nat Rev Microbiol* 12:274-88.
- 681 8. Morse SI, Morse JH. 1976. Isolation and properties of the leukocytosis- and lymphocytosis-
682 promoting factor of *Bordetella pertussis*. *J Exp Med* 143:1483-502.
- 683 9. Hall E, Parton R, Wardlaw AC. 1994. Cough production, leucocytosis and serology of rats
684 infected intrabronchially with *Bordetella pertussis*. *J Med Microbiol* 40:205-13.

- 685 10. Parton R, Hall E, Wardlaw AC. 1994. Responses to *Bordetella pertussis* mutant strains and
686 to vaccination in the coughing rat model of pertussis. *J Med Microbiol* 40:307-12.
- 687 11. Scanlon KM, Snyder YG, Skerry C, Carbonetti NH. 2017. Fatal pertussis in the neonatal
688 mouse model is associated with pertussis toxin-mediated pathology beyond the airways.
689 *Infect Immun* 85.
- 690 12. Stein PE, Boodhoo A, Armstrong GD, Cockle SA, Klein MH, Read RJ. 1994. The crystal
691 structure of pertussis toxin. *Structure* 2:45-57.
- 692 13. Stein PE, Boodhoo A, Armstrong GD, Heerze LD, Cockle SA, Klein MH, Read RJ. 1994.
693 Structure of a pertussis toxin-sugar complex as a model for receptor binding. *Nat Struct*
694 *Biol* 1:591-6.
- 695 14. Weiss AA, Johnson FD, Burns DL. 1993. Molecular characterization of an operon required
696 for pertussis toxin secretion. *Proc Natl Acad Sci U S A* 90:2970-4.
- 697 15. Hazes B, Boodhoo A, Cockle SA, Read RJ. 1996. Crystal structure of the pertussis toxin-
698 ATP complex: a molecular sensor. *J Mol Biol* 258:661-71.
- 699 16. Simon NC, Aktories K, Barbieri JT. 2014. Novel bacterial ADP-ribosylating toxins:
700 structure and function. *Nat Rev Microbiol* 12:599-611.
- 701 17. Katada T, Ui M. 1982. Direct modification of the membrane adenylate cyclase system by
702 islet-activating protein due to ADP-ribosylation of a membrane protein. *Proc Natl Acad Sci*
703 *U S A* 79:3129-33.
- 704 18. West RE, Moss J, Vaughan M, Liu T, Liu TY. 1985. Pertussis toxin-catalyzed ADP-
705 ribosylation of transducin. Cysteine 347 is the ADP-ribose acceptor site. *J Biol Chem*
706 260:14428-30.

- 707 19. Graf R, Codina J, Birnbaumer L. 1992. Peptide inhibitors of ADP-ribosylation by pertussis
708 toxin are substrates with affinities comparable to those of the trimeric GTP-binding
709 proteins. *Mol Pharmacol* 42:760-4.
- 710 20. Weis WI, Kobilka BK. 2018. The molecular basis of G protein-coupled receptor activation.
711 *Annu Rev Biochem* 87:897-919.
- 712 21. Pizza M, Covacci A, Bartoloni A, Perugini M, Nencioni L, De Magistris MT, Villa L,
713 Nucci D, Manetti R, Bugnoli M. 1989. Mutants of pertussis toxin suitable for vaccine
714 development. *Science* 246:497-500.
- 715 22. Littler DR, Ang SY, Moriel DG, Kocan M, Kleifeld O, Johnson MD, Tran MT, Paton AW,
716 Paton JC, Summers RJ, Schembri MA, Rossjohn J, Beddoe T. 2017. Structure-function
717 analyses of a pertussis-like toxin from pathogenic *Escherichia coli* reveal a distinct
718 mechanism of inhibition of trimeric G-proteins. *J Biol Chem* 292:15143-15158.
- 719 23. Putt KS, Hergenrother PJ. 2004. An enzymatic assay for poly(ADP-ribose) polymerase-1
720 (PARP-1) via the chemical quantitation of NAD(+): application to the high-throughput
721 screening of small molecules as potential inhibitors. *Anal Biochem* 326:78-86.
- 722 24. Venkannagari H, Fallarero A, Feijs KL, Lüscher B, Lehtiö L. 2013. Activity-based assay
723 for human mono-ADP-ribosyltransferases ARTD7/PARP15 and ARTD10/PARP10 aimed
724 at screening and profiling inhibitors. *Eur J Pharm Sci* 49:148-56.
- 725 25. Locht C, Keith JM. 1986. Pertussis toxin gene: nucleotide sequence and genetic
726 organization. *Science* 232:1258-64.
- 727 26. Nicosia A, Perugini M, Franzini C, Casagli MC, Borri MG, Antoni G, Almoni M, Neri P,
728 Ratti G, Rappuoli R. 1986. Cloning and sequencing of the pertussis toxin genes: operon
729 structure and gene duplication. *Proc Natl Acad Sci U S A* 83:4631-5.

- 730 27. Moss J, Stanley SJ, Burns DL, Hsia JA, Yost DA, Myers GA, Hewlett EL. 1983.
731 Activation by thiol of the latent NAD glycohydrolase and ADP-ribosyltransferase activities
732 of *Bordetella pertussis* toxin (islet-activating protein). J Biol Chem 258:11879-82.
- 733 28. Finck-Barbançon V, Barbieri JT. 1996. Preferential processing of the S1 subunit of
734 pertussis toxin that is bound to eukaryotic cells. Mol Microbiol 22:87-95.
- 735 29. Sakanyan V, Hulin P, Alves de Sousa R, Silva VA, Hambarzumyan A, Nedellec S,
736 Tomasoni C, Logé C, Pineau C, Roussakis C, Fleury F, Artaud I. 2016. Activation of
737 EGFR by small compounds through coupling the generation of hydrogen peroxide to stable
738 dimerization of Cu/Zn SOD1. Sci Rep 6:21088.
- 739 30. Lüscher B, Bütepage M, Eckeï L, Krieg S, Verheugd P, Shilton BH. 2018. ADP-
740 ribosylation, a multifaceted posttranslational modification involved in the control of cell
741 physiology in health and disease. Chem Rev 118:1092-1136.
- 742 31. Winter K, Zipprich J, Harriman K, Murray EL, Gornbein J, Hammer SJ, Yeganeh N,
743 Adachi K, Cherry JD. 2015. Risk factors associated with infant deaths from pertussis: a
744 case-control study. Clin Infect Dis 61:1099-106.
- 745 32. Guillot S, Descours G, Gillet Y, Etienne J, Floret D, Guiso N. 2012. Macrolide-resistant
746 *Bordetella pertussis* infection in newborn girl, France. Emerg Infect Dis 18:966-8.
- 747 33. Wang Z, Li Y, Hou T, Liu X, Liu Y, Yu T, Chen Z, Gao Y, Li H, He Q. 2013. Appearance
748 of macrolide-resistant *Bordetella pertussis* strains in China. Antimicrob Agents Chemother
749 57:5193-4.
- 750 34. Acquaye-Seedah E, Huang Y, Sutherland JN, DiVenere AM, Maynard JA. 2018.
751 Humanised monoclonal antibodies neutralise pertussis toxin by receptor blockade and
752 reduced retrograde trafficking. Cell Microbiol 20:e12948.

- 753 35. Nguyen AW, Wagner EK, Laber JR, Goodfield LL, Smallridge WE, Harvill ET, Papin JF,
754 Wolf RF, Padlan EA, Bristol A, Kaleko M, Maynard JA. 2015. A cocktail of humanized
755 anti-pertussis toxin antibodies limits disease in murine and baboon models of whooping
756 cough. *Sci Transl Med* 7:316ra195.
- 757 36. Turgeon Z, Jørgensen R, Visschedyk D, Edwards PR, Legree S, McGregor C, Fieldhouse
758 RJ, Mangroo D, Schapira M, Merrill AR. 2011. Newly discovered and characterized
759 antivirulence compounds inhibit bacterial mono-ADP-ribosyltransferase toxins. *Antimicrob*
760 *Agents Chemother* 55:983-91.
- 761 37. Pinto AF, Ebrahimi M, Saleeb M, Forsberg Å, Elofsson M, Schüler H. 2016. Identification
762 of inhibitors of *Pseudomonas aeruginosa* Exotoxin-S ADP-ribosyltransferase activity. *J*
763 *Biomol Screen* 21:590-5.
- 764 38. Locht C, Cieplak W, Marchitto KS, Sato H, Keith JM. 1987. Activities of complete and
765 truncated forms of pertussis toxin subunits S1 and S2 synthesized by *Escherichia coli*.
766 *Infect Immun* 55:2546-53.
- 767 39. Pulliainen AT, Pielles K, Brand CS, Hauert B, Böhm A, Quebatte M, Wepf A, Gstaiger M,
768 Aebersold R, Dessauer CW, Dehio C. 2012. Bacterial effector binds host cell adenylyl
769 cyclase to potentiate *Gas*-dependent cAMP production. *Proc Natl Acad Sci U S A*
770 109:9581-6.
- 771 40. Sastry GM, Adzhigirey M, Day T, Annabhimoju R, Sherman W. 2013. Protein and ligand
772 preparation: parameters, protocols, and influence on virtual screening enrichments. *J*
773 *Comput Aided Mol Des* 27:221-34.

774

775

- 776 41. Friesner RA, Banks JL, Murphy RB, Halgren TA, Klicic JJ, Mainz DT, Repasky MP, Knoll
777 EH, Shelley M, Perry JK, Shaw DE, Francis P, Shenkin PS. 2004. Glide: a new approach
778 for rapid, accurate docking and scoring. 1. Method and assessment of docking accuracy. *J*
779 *Med Chem* 47:1739-49.
- 780 42. Bowers KJ, Chow E, Xu H, Dror RO, Eastwood MP, Gregersen BA, Klepeis JL,
781 Kolossvary I, Moraes MA, Sacerdoti FD, Salmon JoK, Shan Y, Shaw DE. 2006. Scalable
782 algorithms for molecular dynamics simulations on commodity clusters. Proceedings of the
783 ACM/IEEE Conference on Supercomputing (SC06), Tampa, Florida, 2006, November 11-
784 17
- 785 43. Jorgensen WL, Chandrasekhar J, Madura JD, Impey RW, Klein M. 1983. Comparison of
786 simple potential functions for simulating liquid water. *J Chem Phys* 79: 926–935.
- 787 44. Harder E, Damm W, Maple J, Wu C, Reboul M, Xiang JY, Wang L, Lupyan D, Dahlgren
788 MK, Knight JL, Kaus JW, Cerutti DS, Krilov G, Jorgensen WL, Abel R, Friesner RA.
789 2016. OPLS3: A force field providing broad coverage of drug-like small molecules and
790 proteins. *J Chem Theory Comput* 12:281-96.
- 791 45. Martyna GJ, Klein ML, Tuckerman M. 1992. Nose-Hoover chains - the canonical ensemble
792 via continuous dynamics. *J. Chem. Phys.* 97: 2635-2643.
- 793 46. Martyna GJ, Tobias DJ, Klein ML. 1994. Constant-pressure molecular dynamics
794 algorithms. *J Chem Phys* 101: 4177-4189.
- 795 47. Tuckerman M, Berne BJ, Martyna GJ. 1992. Reversible multiple time scale molecular
796 dynamics. *J Chem Phys* 97:1990-2001.
- 797
- 798
- 799

800 **FIGURE LEGENDS**

801

802 **Figure 1. PtxS1 of pertussis toxin. A)** Surface representation of the crystal structure of PtxS1
803 (PDB_1BCP, chain A). The truncated C-terminal fragment and the truncation-uncovered ART
804 active site are shown in yellow and dark grey, respectively. **B)** Possible binding mode of NAD⁺
805 to PtxS1 derived by superimposing the PtxS1 crystal structure (PDB_1BCP, chain A) to the
806 crystal structure of active site mutant of pertussis-like toxin from *E. coli* with bound NAD⁺
807 (PDB_4Z9D). Color-coding of atoms in NAD⁺: yellow, carbon; blue, nitrogen; red, oxygen;
808 magenta, phosphorus.

809

810 **Figure 2. Catalytic activity of rPtxS1. A)** Construct design. rPtxS1 lacks the N-terminal
811 secretion signal (S) as well as part of the C-terminus (C-term). N-terminus of the mature PtxS1
812 starting with Asp35 is classically numbered as the first amino acid of PtxS1. **B)** PageBlue-stained
813 SDS-PAGE gel of SEC-purified rPtxS1. **C)** Representative SEC-MALS result of SEC-purified
814 rPtxS1. **D)** Representative DSF result of SEC-purified rPtxS1. **E)** *In vitro* ADP-ribosylation assay
815 (enzyme-excess condition) for rPtxS1 with NAD⁺-biotin and HEK293T membrane fraction with
816 endogenous level of G α i. Protein-conjugated ADP-ribose-biotin is detected with streptavidin-
817 HRP. **F)** *In vitro* ADP-ribosylation assay (enzyme-excess condition) for rPtxS1 with NAD⁺ and
818 recombinant N-terminally HIS-tagged G α i. Protein-conjugated ADP-ribose is detected with a
819 rabbit polyclonal antibody specific for mono-ADP-ribose (MAR). Same samples were analyzed
820 in three (Fig. 2E) and two (Fig. 2F) parallel membranes, respectively.

821

822

823

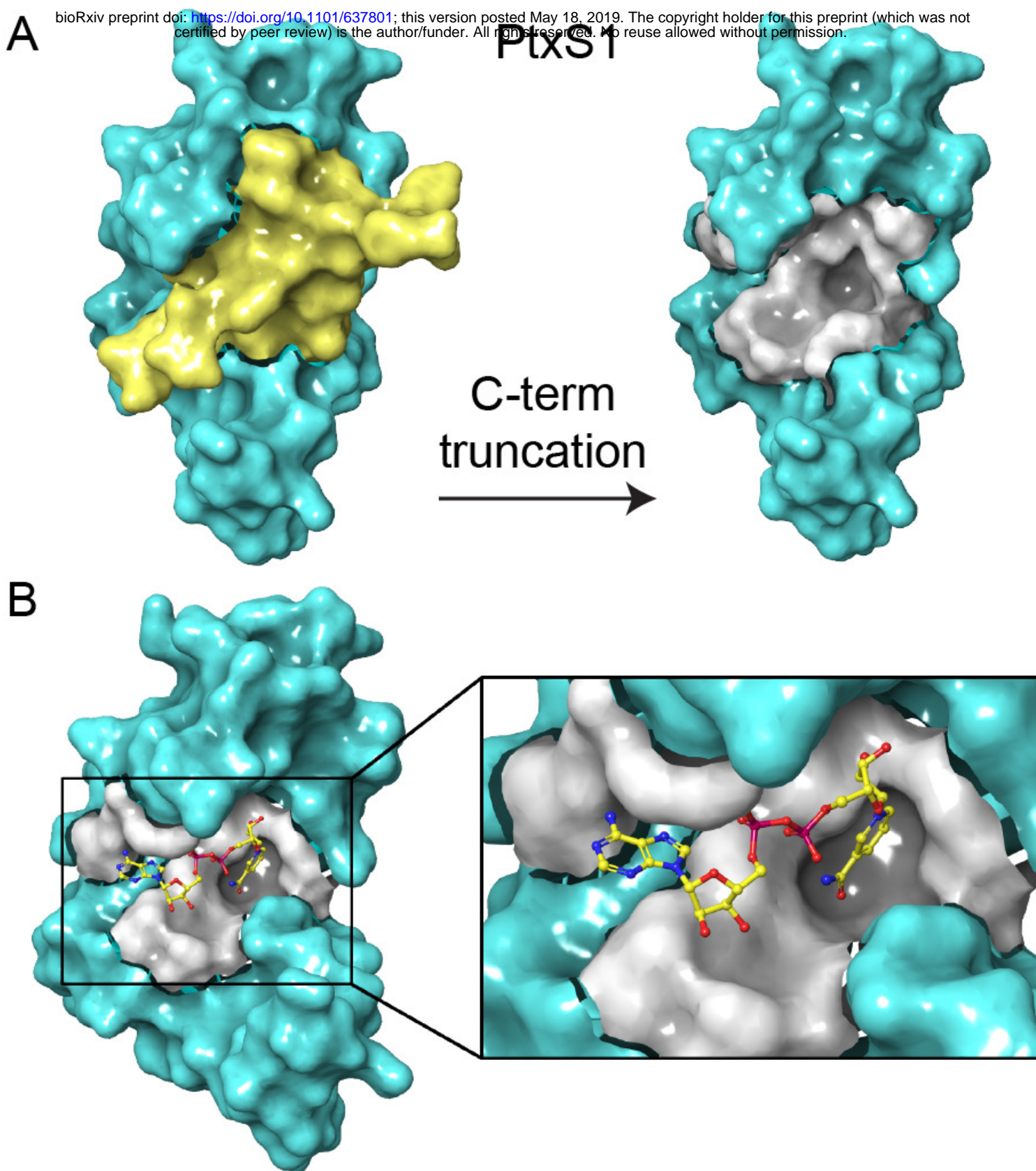
824
825 **Figure 3. Multiwell fluorometric NAD⁺ quantitation assay.** Decrease in fluorescence over
826 time is a measure of NAD⁺-consuming enzymatic activity. **A)** rPtxS1 and rPtxS1-mutant were
827 incubated for 40 min in the presence or for 60 min in the absence of rGai substrate. **B)** Time and
828 concentration dependency of NAD⁺-consuming enzymatic activity of rPtxS1 in the presence of
829 rGai substrate. **C)** Effect of DMSO on NAD⁺-consuming enzymatic activity of rPtxS1 in the
830 presence of rGai substrate. Statistics based on two-tailed Student's t-test two sample equal
831 variance (homoscedastic).

832
833 **Figure 4. Evaluation of primary compound hits from rPtxS1 inhibitor screen.** **A)** *In vitro*
834 ADP-ribosylation assay (substrate-excess condition) for N-terminally HIS-tagged rPtxS1 with
835 NAD⁺-biotin and N-terminally HIS-tagged rGai. Protein-conjugated biotin-ADP-ribose was
836 detected with streptavidin-HRP. The reactions contained 200-fold molar excess of inhibitors over
837 rPtxS1. Compounds marked with asterisks affect rPtxS1 and/or rGai protein integrity, and were
838 therefore excluded from further studies. Same samples were analyzed in two parallel membranes.
839 **B)** IC₅₀-curves of the hit compounds selected based on Fig. 3A data. **C)** Chemical structures of
840 NAD⁺ and hit compounds NSC 228155 and NSC 29193 with < 10 μM IC₅₀-values.

841
842
843
844
845
846
847

848 **Figure 5. Prediction of binding poses of NSC 228155 and NSC 29193 to PtxS1.** Selected
849 binding poses 1 **A)** and 2 **B)** of NSC 228155 and binding poses 1 **C)** and 2 **D)** of NSC 29193 to
850 PtxS1 (PDB_1BCP, chain A), and residues involved in ligand interactions. Binding mode of
851 NAD⁺ to PtxS1 in the corresponding area of the NAD⁺-binding pocket is shown in each panel on
852 the right (see also Fig. 1). Color-coding of atoms in NAD⁺: yellow, carbon; blue, nitrogen; red,
853 oxygen; magenta, phosphorus. Hydrogen bond interactions are shown in dotted lines.

854
855 **Figure 6. Evaluation of NSC 228155 in a living human cell-based assay.** NSC 228155 inhibits
856 pertussis holotoxin-mediated mono-ADP-ribosylation of G α i in living HEK293T cells. **A)** Effect
857 of pertussis holotoxin concentration on mono-ADP-ribosylation of G α i in 2 h incubation with
858 living HEK293T cells. **B)** Effect of NSC 228155 concentration on mono-ADP-ribosylation of
859 G α i in living HEK293T cells. Inhibitors were added 30 min before starting the 2 h holotoxin
860 incubation. Protein-conjugated ADP-ribose is detected with a rabbit polyclonal antibody specific
861 for mono-ADP-ribose (MAR). #Western blot of a parallel membrane with the same Fig. 6B
862 samples, otherwise Fig. 6A and Fig. 6B blots probed, stripped and re-probed in the order of 1)
863 anti-MAR, 2) anti-GAPDH and 3) anti-G α i.



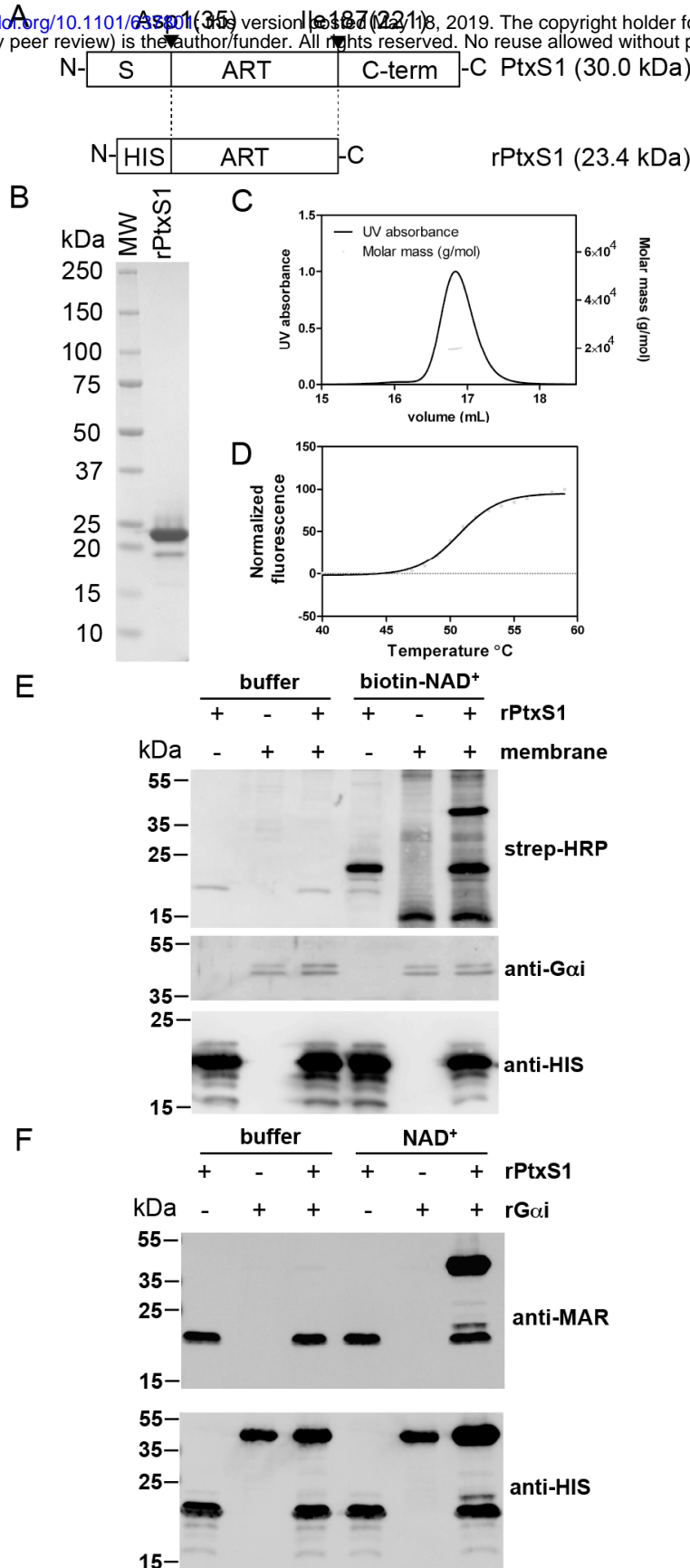


Figure 2. Catalytic activity of rPtxS1. **A)** Construct design. rPtxS1 lacks the N-terminal secretion signal (S) as well as part of the C-terminus (C-term). N-terminus of the mature PtxS1 starting with Asp35 is classically numbered as the first amino acid of PtxS1. **B)** PageBlue-stained SDS-PAGE gel of SEC-purified rPtxS1. **C)** Representative SEC-MALS result of SEC-purified rPtxS1. **D)** Representative DSF result of SEC-purified rPtxS1. **E)** *In vitro* ADP-ribosylation assay (enzyme-excess condition) for rPtxS1 with NAD⁺-biotin and HEK293T membrane fraction with endogenous level of Gai. Protein-conjugated ADP-ribose-biotin is detected with streptavidin-HRP. **F)** *In vitro* ADP-ribosylation assay (enzyme-excess condition) for rPtxS1 with NAD⁺ and recombinant N-terminally HIS-tagged Gai. Protein-conjugated ADP-ribose is detected with a custom in-house rabbit polyclonal antibody specific for mono-ADP-ribose. Same samples were analyzed in three (Fig. 2E) and two (Fig. 2F) parallel membranes, respectively.

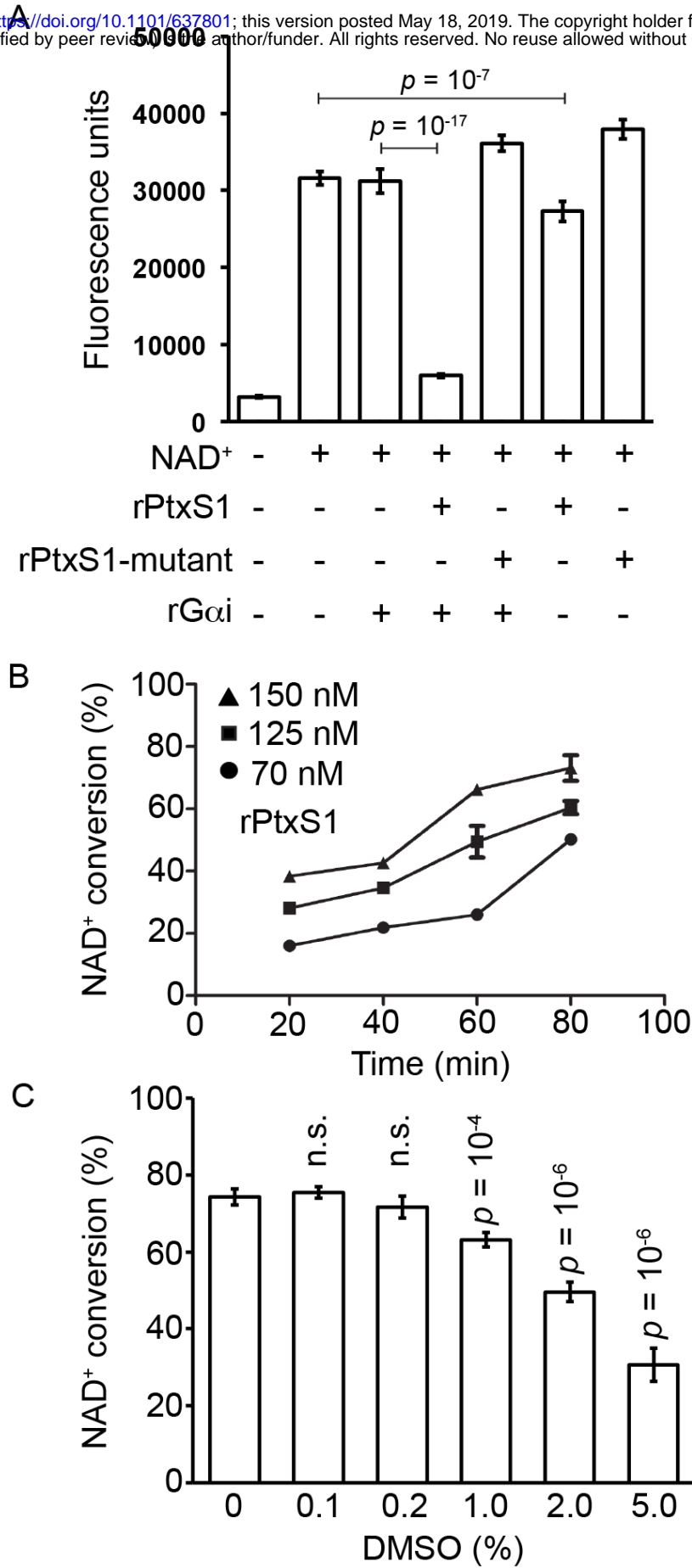


Figure 3. Multiwell fluorometric NAD⁺ quantitation assay. Decrease in fluorescence over time is a measure of NAD⁺-consuming enzymatic activity. **A)** rPtxS1 and rPtxS1-mutant were incubated for 40 min in the presence or for 60 min in the absence of rGai substrate. **B)** Time and concentration dependency of NAD⁺-consuming enzymatic activity of rPtxS1 in the presence of rGai substrate. **C)** Effect of DMSO on NAD⁺-consuming enzymatic activity of rPtxS1 in the presence of rGai substrate. Statistics based on two-tailed Student's t-test two sample equal variance (homoscedastic).

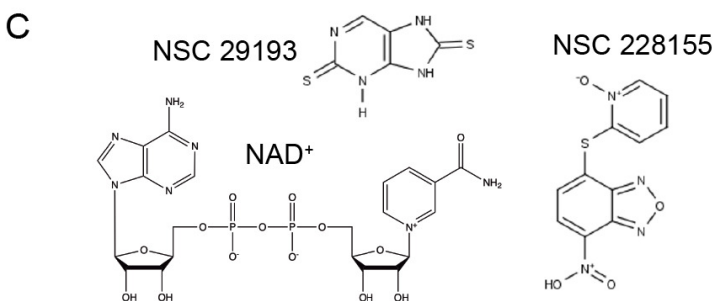
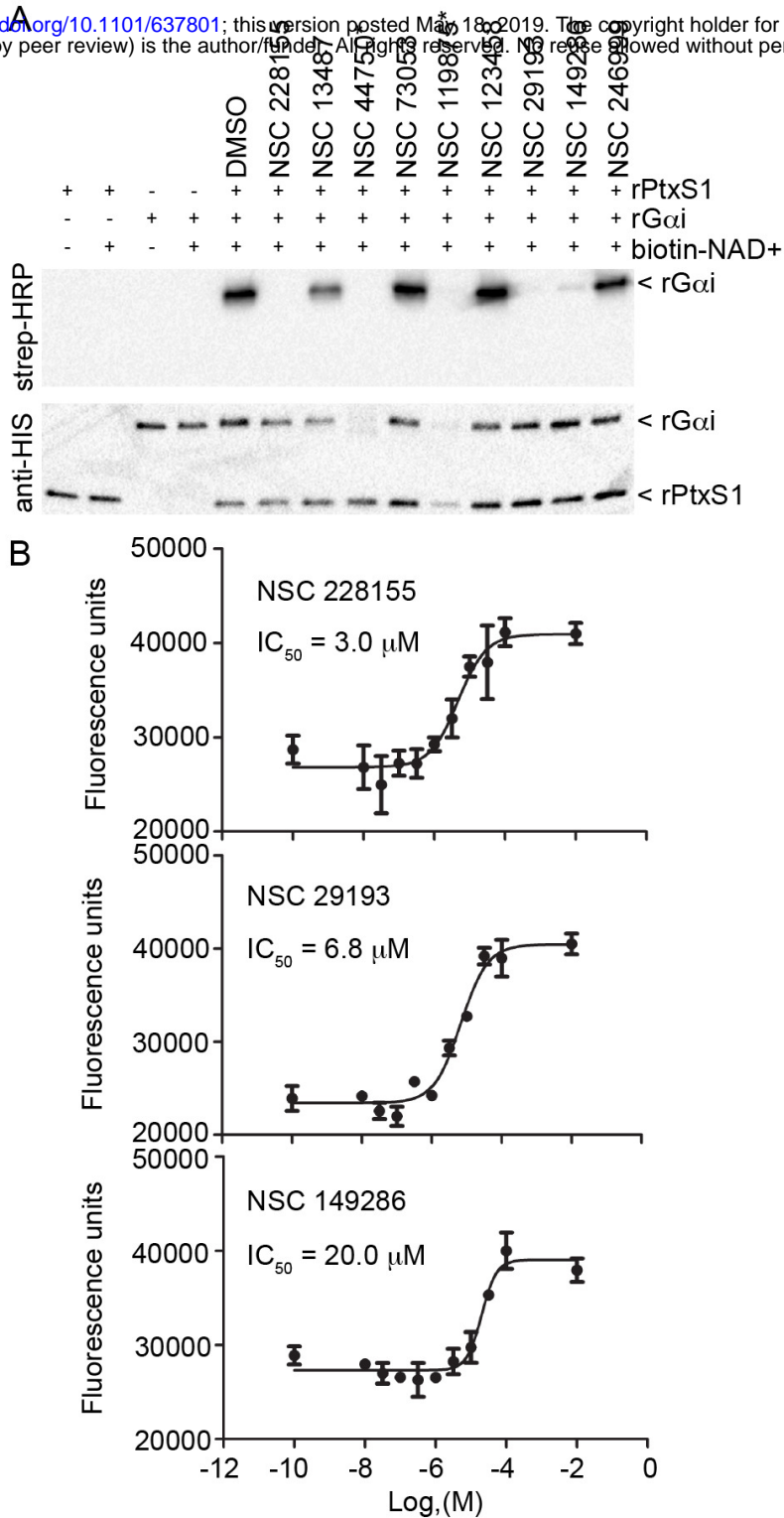


Figure 4. Evaluation of primary compound hits from rPtxS1 inhibitor screen.

A) *In vitro* ADP-ribosylation assay (substrate-excess condition) for N-terminally HIS-tagged rPtxS1 with NAD⁺-biotin and N-terminally HIS-tagged rGai. Protein-conjugated biotin-ADP-ribose was detected with streptavidin-HRP. The reactions contained 200-fold molar excess of inhibitors over rPtxS1. Compounds marked with an asterisk affect rPtxS1 and/or rGai protein integrity, and were therefore excluded from further studies. Same samples were analyzed in two parallel membranes. **B)** IC₅₀-curves of the hit compounds selected based on Fig. 3A data. **C)** Chemical structures of NAD⁺ and hit compounds NSC 228155 and NSC 29193 with < 10 μM IC₅₀-values.

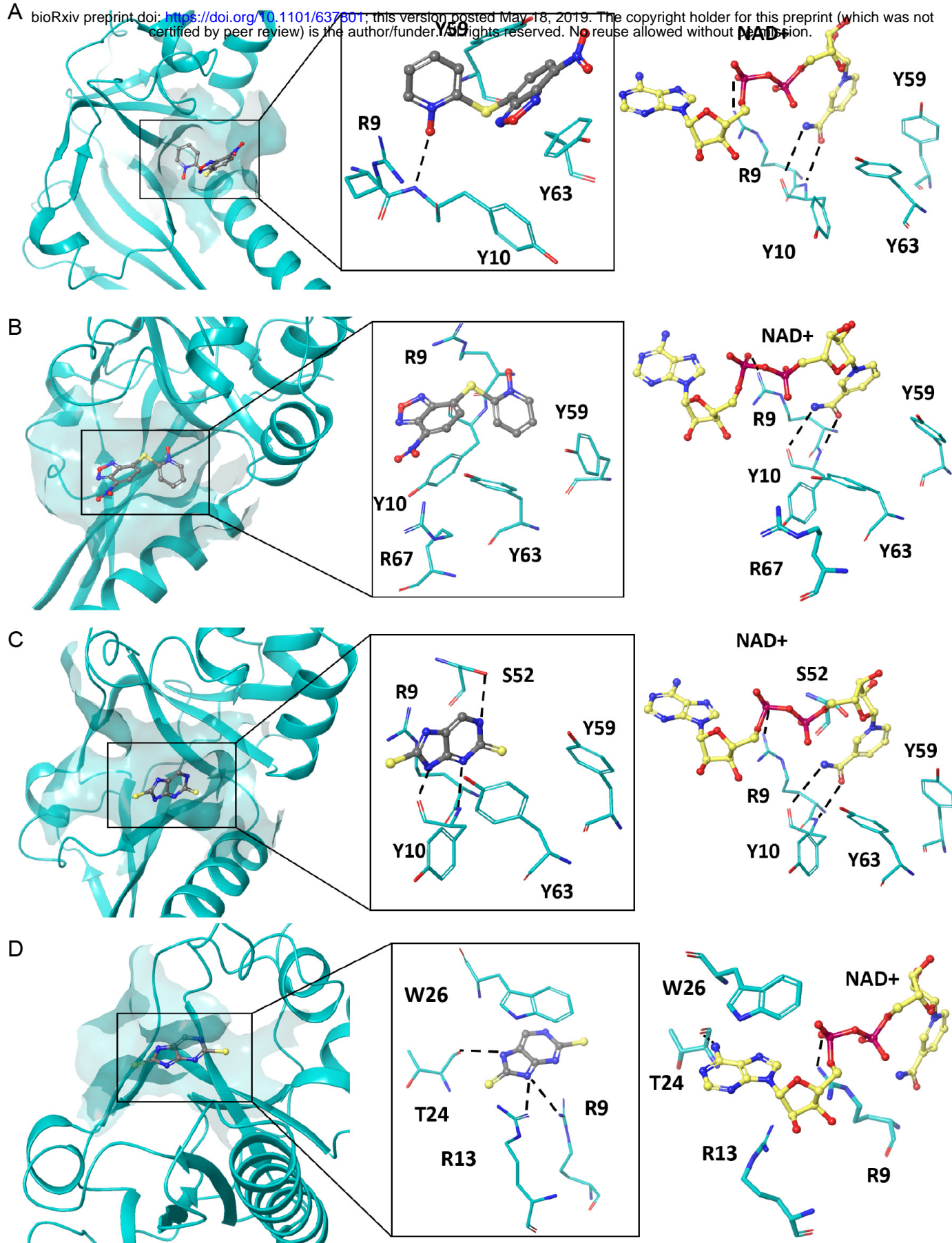


Figure 5. Prediction of binding poses of NSC 228155 and NSC 29193 to PtxS1. Selected binding poses 1 **A**) and 2 **B**) of NSC 228155 and binding poses 1 **C**) and 2 **D**) of NSC 29193 to PtxS1 (PDB_1BCP, chain A), and residues involved in ligand interactions. Binding mode of NAD⁺ to PtxS1 in the corresponding area of the NAD⁺-binding pocket is shown in each panel on the right (see also Fig. 1). Color-coding of atoms in NAD⁺: yellow, carbon; blue, nitrogen; red, oxygen; magenta, phosphorus. Hydrogen bond interactions are shown in dotted lines.

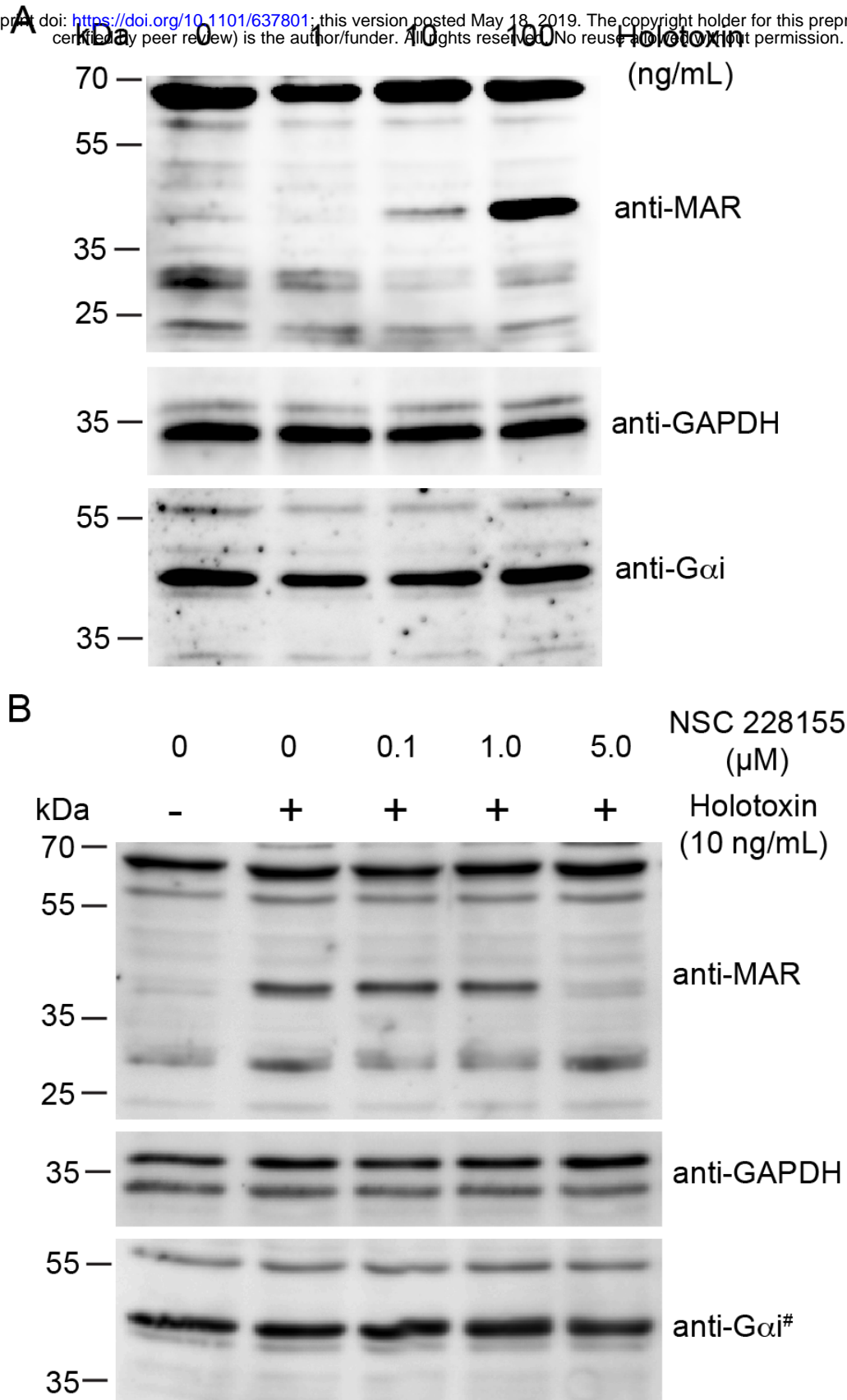


Figure 6. Evaluation of NSC 228155 in a living human cell-based assay. NSC 228155 inhibits pertussis holotoxin-mediated mono-ADP-ribosylation of Gai in living HEK293T cells. **A)** Effect of pertussis holotoxin concentration on mono-ADP-ribosylation of Gai in 2 h incubation with living HEK293T cells. **B)** Effect of NSC 228155 concentration on mono-ADP-ribosylation of Gai in living HEK293T cells. Inhibitors were added 30 min before starting the 2 h holotoxin incubation. Protein-conjugated ADP-ribose is detected with a custom in-house rabbit polyclonal antibody specific for mono-ADP-ribose (MAR). [#]Western blot of a parallel membrane with the same Fig. 6B samples, otherwise Fig. 6A and Fig. 6B blots probed, stripped and re-probed in the order of 1) anti-MAR, 2) anti-GAPDH and 3) anti-Gai.